Research Square

Preprints are preliminary reports that have not undergone peer review.
They should not be considered conclusive, used to inform clinical practice,
or referenced by the media as validated information.

Magnetically recoverable SiW11Cd@CoFe2O4@PANI nanocomposite as an efficient heterogeneous catalyst for oxidative desulfurization of real and model fuels

Mohammad Ali Rezvani

marezvani@znu.ac.ir

University of Zanjan

Mohammad Mohammadi

University of Zanjan

Article

Keywords: polyoxometalate, substituted silicotungstate, cobalt ferrite, polyaniline, oxidative desulfurization

Posted Date: November 3rd, 2026

DOI: https://doi.org/10.21203/rs.3.rs-10983869/v1

License: This work is licensed under a Creative Commons Attribution 4.0 International License.
Read Full License

Additional Declarations: No competing interests reported.

Magnetically recoverable $SiW_{11}Cd@CoFe_2O_4@PANI$ nanocomposite as an efficient heterogeneous catalyst for oxidative desulfurization of real and model fuels

Mohammad Ali Rezvani* and Mohammad Mohammadi

Department of Chemistry, Faculty of Science, University of Zanjan, 451561319, Zanjan, Iran

**Corresponding author: E-mail: marezvani@znu.ac.ir ; Tel./Fax: +98 (24) 3305 2477*

ABSTRACT:

A new inorganic–organic hybrid nanocomposite, $SiW_{11}Cd@CoFe_2O_4@PANI$, was synthesized from the potassium salt of Cd (II)-substituted silicotungstate ($K_6SiW_{11}CdO_{39}$), cobalt ferrite ($CoFe_2O_4$), and polyaniline (PANI) and evaluated as a heterogeneous catalyst for oxidative desulfurization (ODS) process. The synthesized materials were characterized by Fourier-transform infrared spectroscopy (FT-IR), X-ray diffraction (XRD), scanning electron microscopy (SEM), and energy-dispersive X-ray spectroscopy (EDX). The characterization results supported the formation of the hybrid nanocomposite and the incorporation of $K_6SiW_{11}CdO_{39}$ (abbreviated to $SiW_{11}Cd$) within the $CoFe_2O_4$/PANI matrix. The average particle size determined by SEM was approximately 26 nm, while the crystallite size estimated using the Scherrer equation was 21 nm. The catalytic performance of $SiW_{11}Cd@CoFe_2O_4@PANI$ was evaluated using both real gasoline and model fuel containing dibenzothiophene (DBT), benzothiophene (BT) and thiophene (Th). Under optimized conditions, using H_2O_2/CH_3COOH as the oxidizing system, the total sulfur content of real gasoline decreased from 4988 to 208 ppm, corresponding to approximately 96% sulfur removal after 60 min at 35 °C. The enhanced ODS performance is attributed to the combined contribution of the polyoxometalate active sites, magnetic $CoFe_2O_4$ support, and PANI matrix. The nanocomposite could be magnetically recovered and reused for five consecutive reaction cycles while retaining most of its catalytic activity. These results demonstrate the potential of

$SiW_{11}Cd@CoFe_2O_4@PANI$ as a recyclable heterogeneous catalyst for the ODS of real and model fuels under relatively mild conditions

KEYWORDS: polyoxometalate, substituted silicotungstate, cobalt ferrite, polyaniline, oxidative desulfurization.

1. INTRODUCTION

Polyoxometalates (POMs) are well defined metal oxygen clusters, mainly based on Mo, W, and V, that exhibit remarkable redox, acidic, and structural properties, making them attractive catalysts for oxidation and related transformations [1-8]. One of the important features of POMs is their ability to undergo reversible multielectron redox processes while largely retaining their structural integrity. Because of the numerous desirable properties of these compounds, including high thermal stability, high redox properties, and acidic properties, these catalysts have attracted considerable attention and have been extensively studied [9-14]. Transition metal substituted polyoxometalates are often prepared from heteropolyanion cavity compounds. Most lacunary polyoxometalates are of the Keggin-type [15-17]. Polyoxometalates, especially heteropolyacids, have a special place in chemistry as efficient acid and oxidation catalysts [18,19]. However, their catalytic application is limited to bulk inorganic compounds that are less than 10 m^2/g in size. Heteropolyacids have a relatively low surface area compared with the number of their acidic sites, which limits the accessibility of these sites and makes them less effective in catalytic reactions. Consequently, their catalytic activity in vapor–solid-phase reactions is often limited. Also, the high solubility of POMs in polar solvents such as alcohols, water, and ethers make them less suitable for reactions with polar starting materials or products [20,21]. These limitations have motivated extensive efforts to immobilize POMs on suitable organic or inorganic supports in order to enhance catalyst stability, increase the exposed active surface, improve dispersion of the active species, and

facilitate catalyst recovery. Among various supporting materials, cobalt ferrite ($CoFe_2O_4$) has attracted considerable attention. $CoFe_2O_4$ possesses excellent magnetic recoverability, chemical stability and mechanical robustness, making it an attractive support for heterogeneous catalysts [22]. Also, Polyaniline possesses several desirable properties that make it a suitable catalyst support, including high electrical conductivity, abundant amine functional groups, strong interactions with POM species, low density, good flexibility, chemical stability, and low cost [23,24]. Combining magnetic nanoparticles with conductive polymer supports is expected to improve catalyst dispersion, structural stability, and reusability while maintaining high catalytic activity. Although various polyoxometalate-based heterogeneous catalysts and magnetic or polymer-supported systems have previously been investigated for oxidative desulfurization, the present work differs from these reported systems in terms of catalyst composition and design. In particular, the novelty of this study lies in the construction of a multifunctional inorganic–organic hybrid nanocatalyst by integrating a mono-Cd-substituted Keggin-type POM, $K_6SiW_{11}CdO_{39}$ with magnetic $CoFe_2O_4$ nanoparticles and a polyaniline (PANI) matrix. This ternary architecture is designed to combine the oxidation capability of the substituted POM, the magnetic recoverability and structural stability of $CoFe_2O_4$ and the support and dispersion properties of PANI within a single catalytic platform. Although related POM-based, magnetic, and polymer-supported catalysts have been reported, the simultaneous integration of $SiW_{11}Cd$, $CoFe_2O_4$, and PANI for oxidative desulfurization has not been reported in the literature to the best of our knowledge [25–32]. The proposed hybrid structure is therefore expected to provide improved dispersion and accessibility of the catalytic species while facilitating catalyst recovery and reuse. Accordingly, in the present work, $SiW_{11}Cd@CoFe_2O_4@PANI$ was synthesized and evaluated as a recyclable heterogeneous nanocatalyst for the oxidative desulfurization of both model fuel and real gasoline.

The catalytic performance was investigated using an H_2O_2/CH_3COOH oxidation system followed by extraction with CH3CN. The synthesized materials and the final nanocomposite were characterized by FT-IR, XRD, SEM, and EDX analyses. The effects of catalyst dosage, oxidant type, reaction time, and temperature on the ODS performance were investigated, and the recyclability and apparent kinetics of the catalytic process were also evaluated. This study demonstrates the potential of the $SiW_{11}Cd@CoFe_2O_4@PANI$ hybrid as a recyclable catalyst for efficient oxidative desulfurization under relatively mild conditions.

2. EXPERIMENTAL SECTION

2.1. Materials and Methods

DBT, BT, Th, acetonitrile (MeCN), and n-heptane were purchased from Sigma-Aldrich. Silicotungstic acid ($H_3SiW_{12}O_{40}$, ≥99%), cobalt (II) nitrate hexahydrate ($Co(NO_3)_2 \cdot 6H_2O$), iron (III) nitrate nonahydrate ($Fe(NO_3)_3 \cdot 9H_2O$), and hydrochloric acid (HCl, 30%) were purchased from Merck Chemical Group. Also, hydrogen peroxide (H_2O_2, 30%), cetyltrimethylammonium bromide (CTAB, ≥99%), glacial acetic acid (AcOH, ≥100%), and ethanol (C_2H_5OH, ≥96%) were obtained from Fluka. The ODS experiments were performed using a real gasoline sample with a density of 0.7988 g ml^{-1} at 15 °C, a total sulfur content of 0.4988 wt%, and a mercaptan concentration of 98 ppm.

The Fourier-transform infrared (FT-IR) spectra were recorded using a Bruker Tensor 27 spectrometer equipped with potassium bromide (KBr) pellets over the range of 400-4000 cm^{-1}. For the analysis of the crystal structure, X-ray Diffraction (XRD) patterns were recorded using a Bruker D8 Advance instrument using Cu Kα radiation. Furthermore, the particle size and surface characteristics of the materials were examined using a Philips XL30 scanning electron microscopy (SEM) equipped with an Energy Dispersive X-ray (EDX) detector (voltage of 10.00 kV).

2.2. Preparation of mono Cd-substituted Keggin-type POM ($K_6SiW_{11}CdO_{39}$)

0.2 g of $H_3SiW_{12}O_{40}$ was dissolved in the minimum amount of distilled water, and the pH of the solution was measured to be approximately 1.5. 1 M sodium hydroxide was added dropwise until the pH stabilized at 4.5-4.8. After that, a 0.2 M solution of $Cd(NO_3)_2$ salt (0.48 g in 10 mL) was slowly added to the $H_3SiW_{12}O_{40}$ solution at 80 °C. Saturated KCl solution was slowly added to the above solution (potassium ions acted as counter-cations, replacing the hydrogen ions in the polyoxometalate). Finally, the reaction product was dried at room temperature.

2.3. Synthesis of cobalt ferrite nanoparticles ($CoFe_2O_4$)

0.2 M solution of $Fe(NO_3)_3.9H_2O$ (0.8 g in 10 mL water) and 0.1 M solution of $Co(NO_3)_2.6H_2O$ (0.35 g in 10 mL) were mixed under magnetic stirring, designated as solution A. Then, a 0.1 M CTAB solution (0.36 g in 10 mL deionized water) was added to solution A and stirred for 10 min. 0.2 M sodium hydroxide solution was added to the solution A as a precipitating agent until the pH of the solution reached 9. At the end, the color of the solution turned dark brown, indicating the successful progress of the reaction. The obtained precipitate was washed with water and ethanol. The precipitate was dried at 100 °C for 12 h and then calcined at 400 °C for 2 h.

2.4. Synthesis of polyaniline (PANI)

0.5 mL of aniline was dispersed in 10 mL of deionized water and this solution was designated as solution A. 1.1 g of $(NH_4)_2S_2O_8$ was dissolved in 5 mL of distilled water in a separate vessel and designated as solution B. Now solution B was added dropwise to the aniline solution (solution A). The resulting mixture was kept in an ultrasonic bath for 10 min to make it completely homogeneous. The resulting homogeneous solution was stirred continuously for 30 min at 500 rpm using a magnetic stirrer to facilitate the polymerization process.

2.5. Synthesis of nanocomposite $SiW_{11}Cd@CoFe_2O_4$

0.05 g of polyoxometalate ($K_6SiW_{11}CdO_{39}$) was dissolved in 10 mL of distilled water, called solution A. 0.1 g of $CoFe_2O_4$ was dissolved in 10 mL of distilled water. The $CoFe_2O_4$ suspension was then added to solution A, sonicated for 2 h, and centrifuged for 30 min. Finally, it was placed in an oven at 75 °C for 2-3 h.

2.6. Synthesis of nanocomposite ($SiW_{11}Cd@CoFe_2O_4$@PANI)

0.05 g of the synthesized $SiW_{11}Cd@CoFe_2O_4$ was dissolved in 5 mL of distilled water. The solution was placed in an ultrasonic bath for 10 min to prepare a uniform solution. During the formation of polyaniline, the $SiW_{11}Cd@CoFe_2O_4$ solution was mixed in the polyaniline solution for 2 h. The precipitated material was filtered and washed with 10 mL of distilled water and 10 mL of ethanol. Finally, the product was dried at 80 °C for 3 h.

2.7. Desulfurization process by $SiW_{11}Cd@CoFe_2O_4$@PANI nanocatalyst

The desulfurization experiments for real gasoline and model fuel were conducted under the following reaction conditions: First, to prepare a model oil solution with a certain concentration of total sulfur, the required amount of dibenzothiophene (DBT) was calculated and dissolved in a certain volume of organic solvent (n-heptane). The concentration of each sulfur compound in the model fuel was set to 500 ppmw. Then, 50 mL of real gasoline or model fuel was added to the flask in a water bath at 35 °C. After preparation of the reaction medium, 0.1 g of the synthesized $SiW_{11}Cd@CoFe_2O_4$@PANI nanocatalyst was added, and the suspension was vigorously stirred to obtain a homogeneous catalytic system. Subsequently, an oxidant composed of CH_3COOH and H_2O_2 (1:2, v/v) was introduced dropwise into the reaction mixture. The ODS process was performed at 35 °C for 1 h. Following the reaction, the system was cooled to room temperature and transferred to a separatory funnel. The resulting sulfones were then removed from the gasoline

phase by liquid–liquid extraction with 10 mL of acetonitrile. After adding 10 mL of acetonitrile and shaking, two phases were formed, with the organic phase was located above the aqueous phase. The total sulfur content of the gasoline before and after the reaction was determined by standard tests (ASTM D-4294). The efficiency of removing sulfur compounds from the gasoline sample was calculated based on equation (1), where C_0 and C are the initial and final concentrations, respectively.

$$\text{Sulfur removal efficiency (\%)} = \left[\frac{C_0 - C}{C_0}\right] \times 100 \quad (1)$$

3. RESULTS AND DISCUSSION

3.1. FT-IR spectra

To evaluate the correct synthesis of the $SiW_{11}Cd@CoFe_2O_4@PANI$ nanocomposite, the vibrations and interactions of different bonds in the range of 400-4000 cm^{-1} were analyzed using an FT-IR spectrometer (Figure 1). The different spectra for the synthesized compounds, including the substrates, the *mono* Cd-substituted Keggin-type polyoxometalate, and the final nanocomposite ($SiW_{11}Cd@CoFe_2O_4@PANI$) are shown in Figure 1. Thus, Figure 1a corresponds to the spectrum of the polyaniline substrate, the spectrum Figure 1b to the $CoFe_2O_4$ substrate, Figure 1c to the $SiW_{11}CdO_{39}$ polyoxometalate, Figure 1d to the $SiW_{11}CdO_{39}$ polyoxometalate loaded on the $CoFe_2O_4$ substrate, and finally Figure 1e to the final $SiW_{11}Cd@CoFe_2O_4@PANI$ nanocomposite. According to Figure 1a, the peaks obtained at 1580 and 1490 cm^{-1} are related to the ring vibrations of quinoid and benzenoid, respectively [24]. Also, the absorption band observed at 1305 cm^{-1} is related to the stretching vibrations of the second type of amine. In addition, the long and strong peak obtained at 1143 cm^{-1} confirms the bond vibrations of the -NH+= structure in the polymer units, which include the structures Q=NH+-B and B-NH+-B. Since these peaks indicate the presence of positively charged centers in the polymer, polyaniline can serve as an electrostatically

favorable support for various negatively charged species (polyoxoanions) [24]. The peaks identified in Figure 1b for the $CoFe_2O_4$ compound at 640 and 431 cm^{-1} are related to the vibrations of the Fe-O and Co-O bonds, respectively [22]. In this way, the first frequency is related to the stretching vibrations of the tetrahedral bonds and the second frequency is related to the stretching vibrations of the octahedral metal-oxygen bonds [18], which together indicate the formation of a spinel structure [18]. Next, we see the index peaks and fingerprint region of the mono Cd-substituted Keggin-type polyoxometalate (983, 934, 874, 772 cm^{-1}) in Figure 1c, which are related to the stretching vibrations of the Si-O tetrahedral oxygen, the W=O terminal oxygen vibration, W-Oc-W (shared corner bridge oxygen) and W-Od-W (shared edge bridge oxygen), respectively [22]. The very broad peak at 3483 cm^{-1} is also attributed to the water molecule [15]. The $CoFe_2O_4$ material in the spectrum Figure 1d shows the index peak but with a slight shift (600 cm^{-1}) as a substrate. Also, the peaks of the POM index can be observed at frequencies of 1055, 994, 954 and 908 cm^{-1} with a slight shift, which indicates the presence of both materials and the interaction between them in the designed composition ($SiW_{11}Cd@CoFe_2O_4$). Finally, for the $SiW_{11}Cd@CoFe_2O_4@PANI$ nanocomposite, all the frequencies related to the polyaniline substrate (1590, 1502, 1292 and 1118 cm^{-1}), $SiW_{11}Cd$ polyoxometalate (1044, 908, 883 and 858 cm^{-1}) and $CoFe_2O_4$ substrate (616 cm^{-1}) can be found with a slight shift in the spectrum Figure 1e, which is a confirmation of the correct synthesis of the nanocomposite.

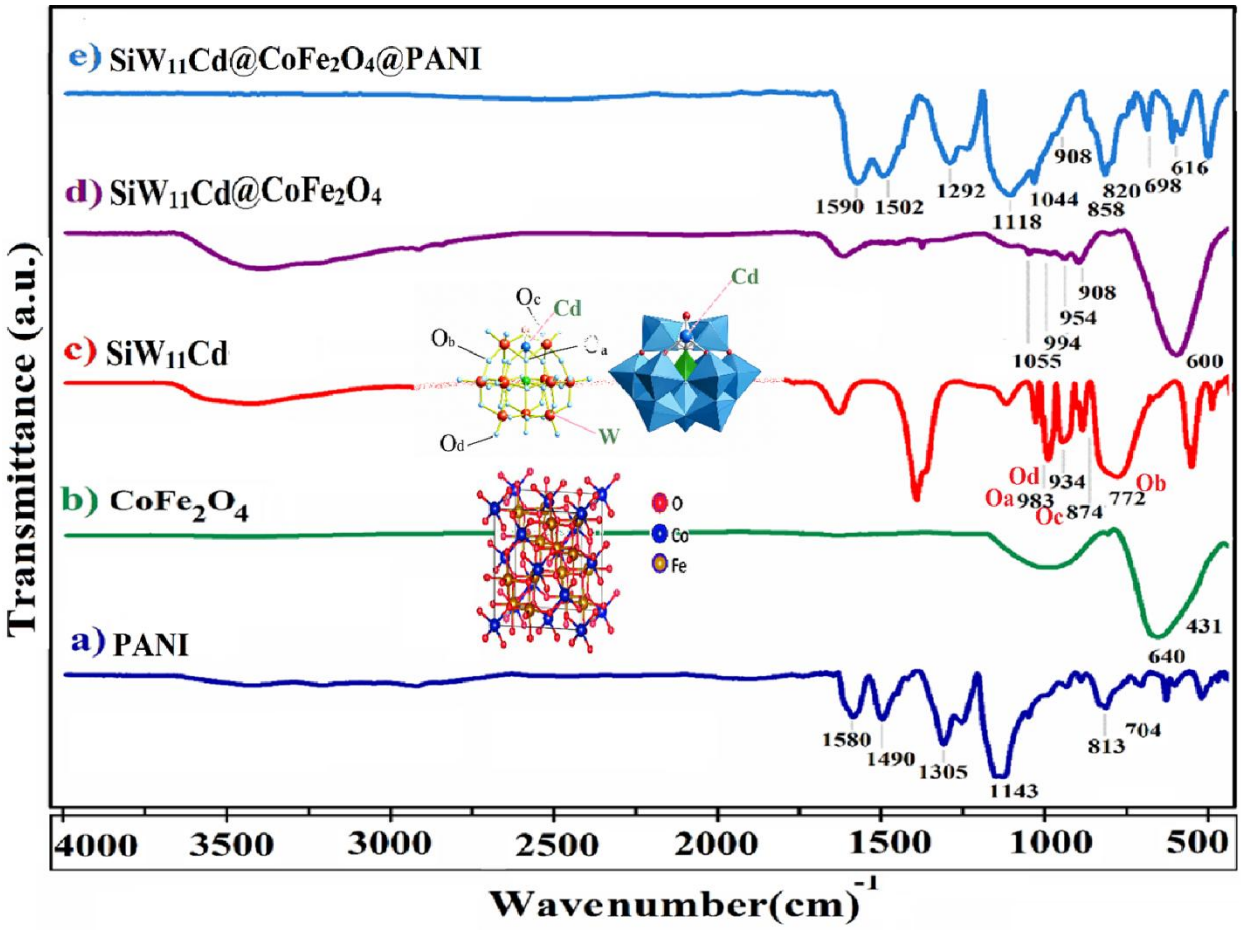


Figure 1. FT-IR spectra of (a) PANI, (b) $CoFe_2O_4$, (c) $SiW_{11}Cd$, (d) $SiW_{11}Cd@CoFe_2O_4$ and (e) $SiW_{11}Cd@CoFe_2O_4$@PANI nanocomposite.

3.2. UV–Vis spectroscopic analysis

The UV–Vis absorption spectra of $SiW_{11}Cd$, PANI, $CoFe_2O_4$, and the $SiW_{11}Cd@CoFe_2O_4$@PANI nanocomposite are shown in Figure 2. The pristine $SiW_{11}Cd$ exhibits two characteristic absorption bands at approximately 202 and 265 nm, which are typical of the electronic transitions associated with the Keggin-type POM framework. The intense absorption band in the deep UV region can be primarily attributed to ligand to metal charge transfer (LMCT) transitions from the O2p orbitals of the oxygen ligands to the vacant W 5d orbitals of W(VI). In particular, transitions involving the

terminal W-O bonds contribute significantly to the high energy UV absorption. The absorption feature observed at approximately 265 nm can be associated with lower energy LMCT transitions within the W-O framework, particularly those involving bridging oxygen atoms between adjacent tungsten centers [24]. The distinction between these transitions reflects the different electronic environments of terminal and bridging oxygen atoms in the Keggin-type POM structure. Importantly, W(VI) in $SiW_{11}Cd$ possesses a d^0 electronic configuration; therefore, the observed UV absorption bands cannot be assigned to conventional W(VI) d-d transitions. Instead, they predominantly arise from charge transfer processes involving the oxygen to tungsten framework. The incorporation of a single Cd center into the lacunary Keggin-type framework can further perturb the local electronic structure and modify the electron density distribution around the neighboring W-O units. Consequently, the LMCT transitions are sensitive to the structural environment created by the Cd-substituted Keggin-type framework. For PANI, an absorption band is observed at approximately 219 nm, which can mainly be assigned to the $\pi \rightarrow \pi^*$ transition of the conjugated aromatic backbone. This transition originates from excitation of π electrons within the delocalized benzene/quinoid related conjugated system and confirms the presence of an extended π-electron system in PANI [24]. The relatively broad absorption extending toward longer wavelengths is also consistent with the electronic delocalization and heterogeneous oxidation states characteristic of conducting polyaniline. The $CoFe_2O_4$ sample exhibits strong absorption in the UV region, with a characteristic feature around 210 nm, followed by a broad absorption tail extending into the visible region. The UV absorption can be associated with charge-transfer transitions involving the O2p orbitals and the unoccupied electronic states of Fe and Co cations within the spinel ferrite lattice [18]. The broad absorption extending toward the visible region is characteristic of the complex electronic structure of $CoFe_2O_4$ and can be related to the presence of

multiple metal–oxygen electronic states and interionic charge-transfer processes. Interestingly, after integration of the three components, the $SiW_{11}Cd@CoFe_2O_4@PANI$ nanocomposite exhibits a modified absorption profile, with a distinct absorption feature appearing at approximately 239 nm. The shift in the absorption maximum relative to the characteristic bands of the pristine $SiW_{11}Cd$, PANI, and $CoFe_2O_4$ components, together with the changes in absorption intensity and band broadening, indicates a significant modification of the electronic environment upon heterostructure formation. This spectral evolution can be attributed to interfacial electronic coupling and charge redistribution among the $SiW_{11}Cd$, $CoFe_2O_4$, and PANI components. In particular, the electron-accepting nature of the W(VI)-based polyoxometalate, the semiconducting character of $CoFe_2O_4$, and the π-conjugated electronic structure of PANI provide favorable conditions for interfacial charge-transfer interactions. Such interactions can alter the energy levels of the individual components and consequently modify the corresponding LMCT and π–π* transitions. The appearance of the absorption band around 239 nm can therefore be considered a consequence of the altered electronic structure and strong interfacial interactions within the ternary heterostructure. Overall, the observed changes in the UV–Vis absorption profile provide strong spectroscopic evidence for the successful integration of $SiW_{11}Cd$, $CoFe_2O_4$, and PANI and the establishment of electronic communication between the constituent phases

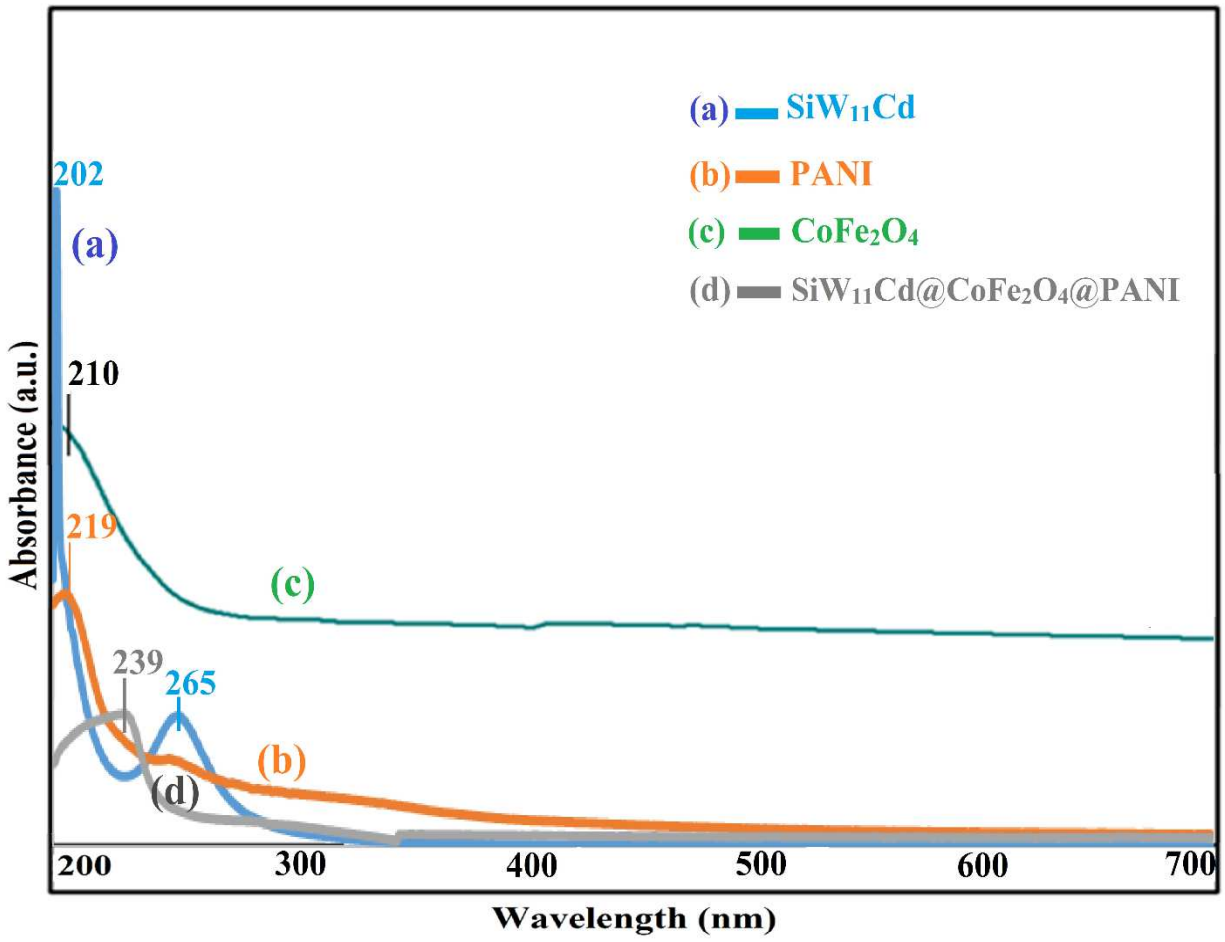


Figure 2. UV–Vis absorption spectra of (a) $SiW_{11}Cd$, (b) PANI, (c) $CoFe_2O_4$, and (d) $SiW_{11}Cd@CoFe_2O_4@PANI$ nanocomposite.

3.3. XRD Data

The crystal structure and different phases of the synthesized compounds were investigated by XRD analysis at $10° \leq 2\theta \leq 80°$. Figure 3a shows the XRD pattern of the $CoFe_2O_4$ support, exhibiting distinct and sharp diffraction peaks assigned to the (111), (220), (311), (222), (400), (422), (511), (440), (531), (620), and (533) crystal planes. The observed reflections at 2θ values of 18.20, 30.28, 36.19, 37.54, 44.15, 53.35, 57.35, 65.62, 66.81, 72.11 and 74.63°, are consistent with the crystalline spinel structure of $CoFe_2O_4$ and the corresponding JCPDS reference card [22]. The $K_6SiW_{11}CdO_{39}$

polyoxometalate (Figure 3b) shows a pattern with sharp and well-spaced peaks (at angles of 28.68, 40.86, 50.40, 58.91, 66.69, and 72.91°), indicating its highly crystalline structure. In the XRD pattern of $SiW_{11}Cd@CoFe_2O_4$ (Figure 3c), the characteristic reflections of $CoFe_2O_4$ are retained, while the diffraction features associated with $K_6SiW_{11}CdO_{39}$ are also observed, indicating the coexistence of both components in the hybrid material. Also, Figure 3e shows the loading of the $SiW_{11}Cd@CoFe_2O_4$ compound on PANI. Polyaniline has an amorphous structure and its crystallinity is relatively low and has a broad-spectrum pattern (Figure 3e), hence the two broad peaks observed at angles of 2θ of 23 and 27° are related to polyaniline [24]. These broad peaks are related to parallel and alternating chains of polyaniline, which leads to the creation of an amorphous and disordered structure [24]. Also, considering the reduction and broadening of the $SiW_{11}CdO_{39}$ peaks and the observation of a larger number of $CoFe_2O_4$ substrate peaks along with the single polyaniline peak, it is obtained that the $SiW_{11}Cd@CoFe_2O_4$ compound is dispersed and stabilized on the PANI substrate, which confirms the appropriate substrate and ultimately the correct synthesis of the $SiW_{11}Cd@CoFe_2O_4@PANI$ nanocomposite. Also, the crystallite size for this nanocomposite was calculated to be 21 nm by the Scherrer equation and X'pert software. The Scherrer equation is the crystallite size estimated from the width of the X-ray diffraction peak at half of its maximum intensity.

$$D_p = 0.94\lambda/FWHM\ \cos\theta \quad (2)$$

Where FWHM represents the width of a peak in a graph measured at half of its maximum value, λ is the X-ray wavelength (λ=0.15406 nm), and θ is Bragg angle. This estimation reflects the size of coherently diffracting domains rather than the actual particle size, which may be larger due to agglomeration effects.

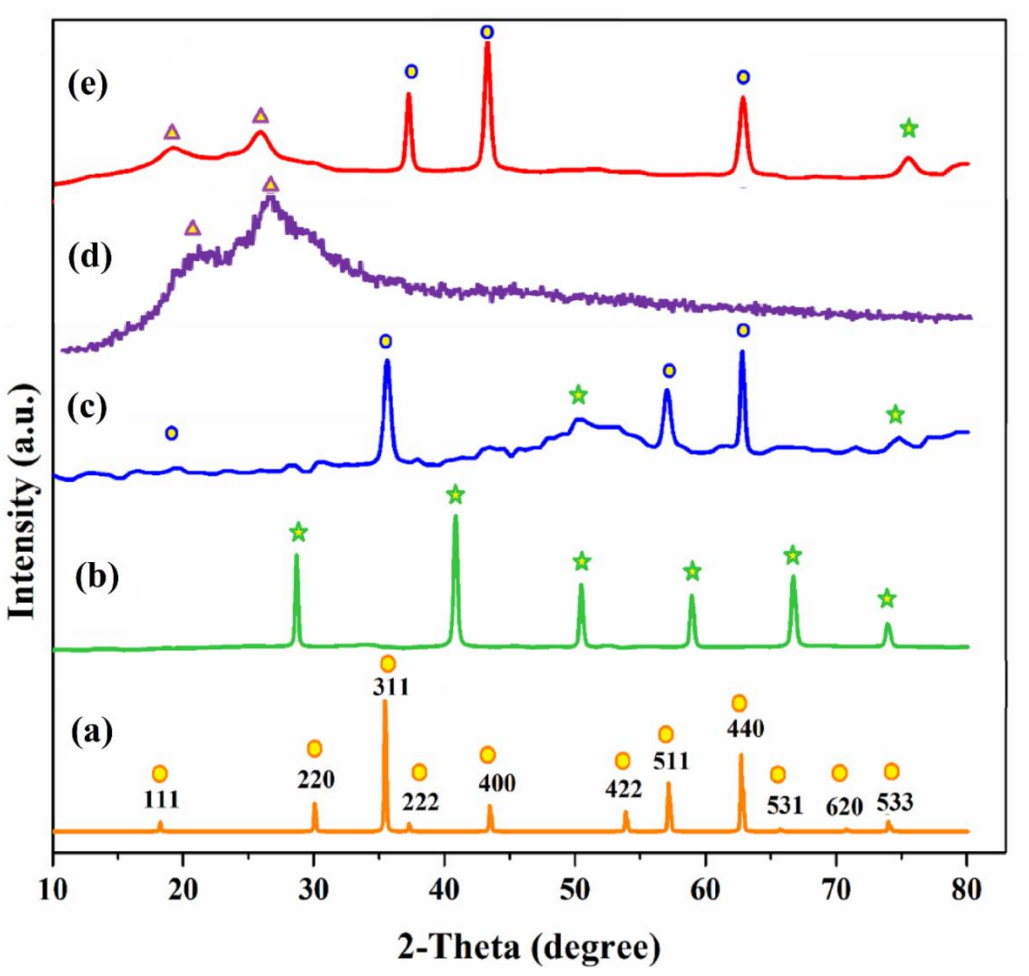


Figure 3. XRD patterns of (a) $CoFe_2O_4$, (b) $SiW_{11}Cd$, (c) $SiW_{11}Cd@CoFe_2O_4$, (d) PANI and (e) $SiW_{11}Cd@CoFe_2O_4@PANI$ nanocomposite.

3.4. SEM

Figure 3 shows the morphology of the synthesized materials and $SiW_{11}Cd@CoFe_2O_4@PANI$ nanocomposite. The morphology of the synthesized samples and the dispersion of active components in the composite were evaluated by SEM analysis. SEM images revealed the surface of the $SiW_{11}Cd@CoFe_2O_4@PANI$ nanocatalyst is not smooth and shows that the synthesized catalytic particles exhibit a spherical morphology with nanoscale dimensions, which was consistent with the successful loading of $SiW_{11}Cd$ onto the $CoFe_2O_4$ and PANI substrates. The

image is reported at a scale of 200 nm. The SEM images of the synthesized compounds and the final nanocomposite were prepared to determine the morphology, proper synthesis, and the loading of the $SiW_{11}Cd$ on the ceramic and PANI (Figure 4). Figure 4a shows the morphology of $K_6SiW_{11}Cd$, which has a lump-like or rock-like structure, is non-uniform and irregular. Figure 4b shows the morphology of the $CoFe_2O_4$ nanoceramic, which is spherical, uniform, and nano-sized. When the $SiW_{11}CdO_{39}$ was completely stabilized and dispersed on the $CoFe_2O_4$ substrate and the $SiW_{11}CdO_{39}@CoFe_2O_4$ nanocomposite was formed, the $CoFe_2O_4$ still maintained its morphology, as shown in Figure 4c. The presence of the initial structure and morphology of $CoFe_2O_4$ without any change in the nanocomposition of $SiW_{11}Cd@CoFe_2O_4$ and then after the $SiW_{11}Cd@CoFe_2O_4$ substrate on PANI can be observed, as well as the presence of POM in Figure 4c and e. The morphology of polyaniline polymer is in the form of a polymer sponge as seen in Figure 4d. However, when $SiW_{11}CdO_{39}$ and $CoFe_2O_4$ are added, the morphology undergoes a remarkable change, characterized by a significant increase in roughness. The uniform morphology observed for the nanocomposite $SiW_{11}Cd@CoFe_2O_4@PANI$, as shown in Figure 4e, it is considered the result of the effective dispersion of POM and $CoFe_2O_4$ particles on the surface of PANI polymer. The homogeneous distribution of $SiW_{11}Cd$ and $CoFe_2O_4$ nanoparticles on the PANI matrix increases the accessibility of active sites and minimizes nanoparticle aggregation, which is likely responsible for the observed increase in catalytic activity during ODS. Furthermore, according to Figure 4f, which shows the histogram of particle distribution, the average size of the nanoparticles was found to be 26 nm.

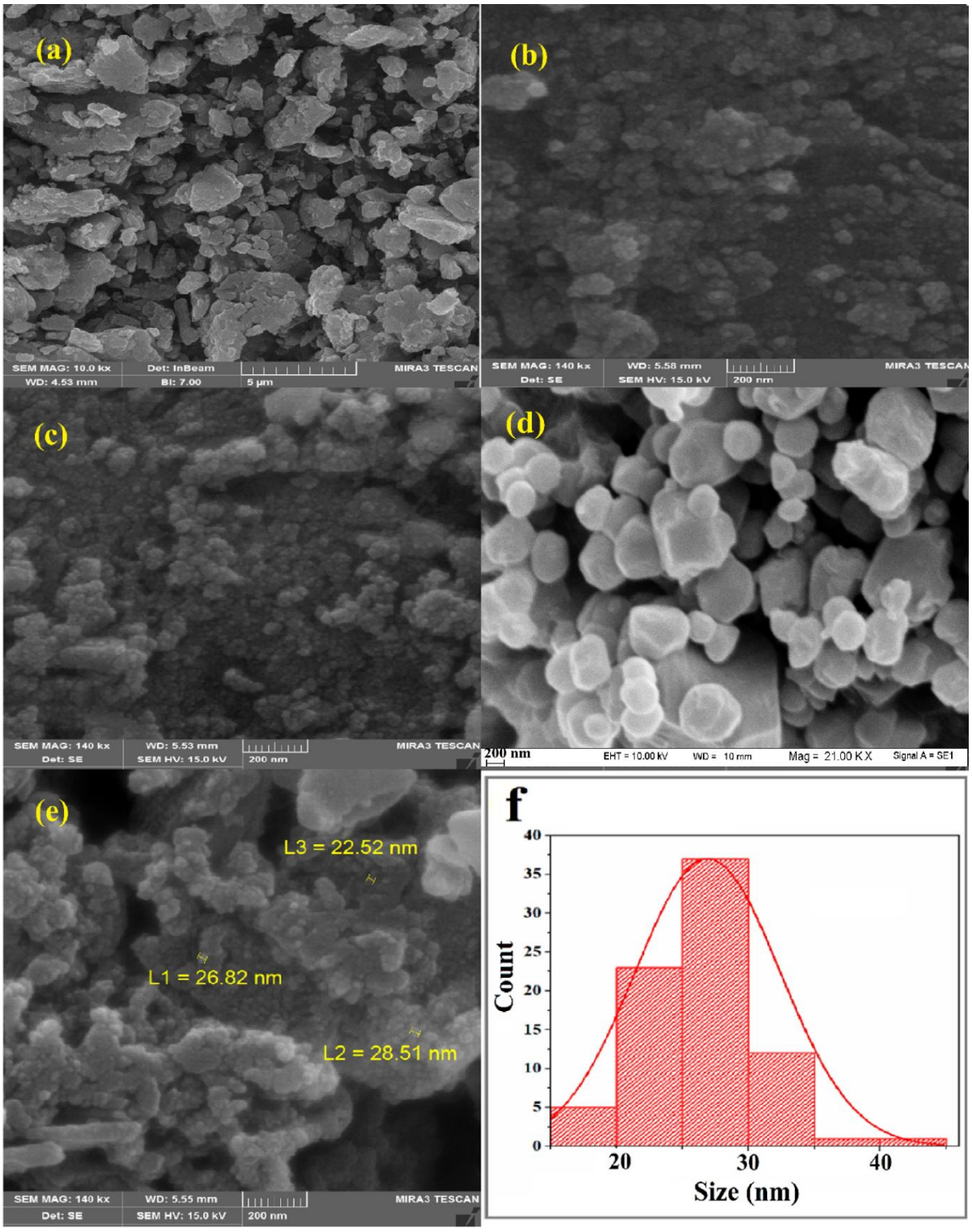
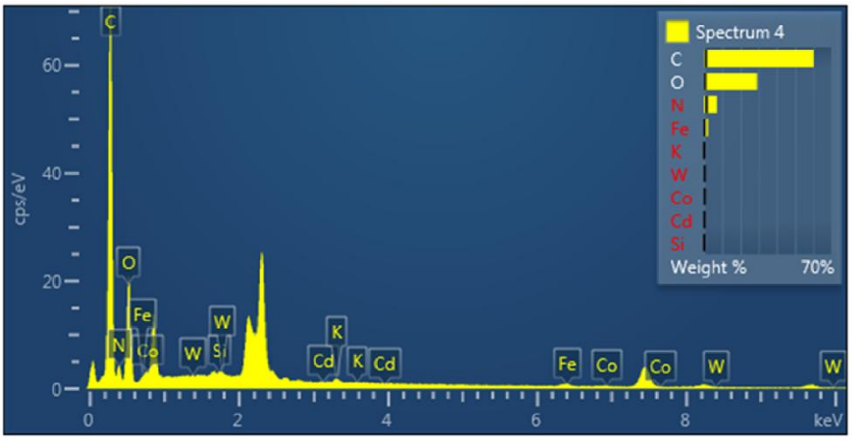


Figure 4. FE-SEM images of (a) $SiW_{11}Cd$, (b) $CoFe_2O_4$, (c) $SiW_{11}Cd@CoFe_2O_4$, (d) PANI [24], (e) $SiW_{11}CdO_{39}@CoFe_2O_4@PANI$, and histogram diagram of the nanocomposite.

3.5. EDX

EDX analysis was employed to identify the different constituent elements in the synthesized nanocomposite $SiW_{11}Cd@CoFe_2O_4@PANI$, which can be seen in Figure 5. Quantitative analysis using EDX has confirmed that the synthesized nanocomposite ($SiW_{11}Cd@CoFe_2O_4@PANI$) contains all the expected constituent elements including C, N, O, Si, W, Cd, Fe, K, and Co. The estimated proportions (measured in weight percent) of these elements are approximately 60.11, 7.25, 29.12, 0.04, 0.45, 0.14, 2.02, 0.61 and 0.25%, respectively. Based on the findings mentioned above, it can be accurately inferred that almost all the components of $SiW_{11}Cd$ and $CoFe_2O_4$ were detected after blending with PANI.



Element	Line Type	Apparent Concentration	k Ratio	Wt%	Wt% Sigma	Atomic %
C	K series	21.76	0.21758	60.11	0.97	67.60
N	K series	2.85	0.00507	7.25	1.33	6.99
O	K series	10.64	0.03580	29.12	0.55	24.59
Si	K series	0.02	0.00016	0.04	0.07	0.02
K	K series	0.30	0.00254	0.61	0.09	0.21
Fe	K series	0.75	0.00755	2.02	0.23	0.49
Co	K series	0.09	0.00092	0.25	0.26	0.06
Cd	L series	0.05	0.00050	0.14	0.20	0.02
W	M series	0.15	0.00152	0.45	0.23	0.03
Total:				100.00		100.00

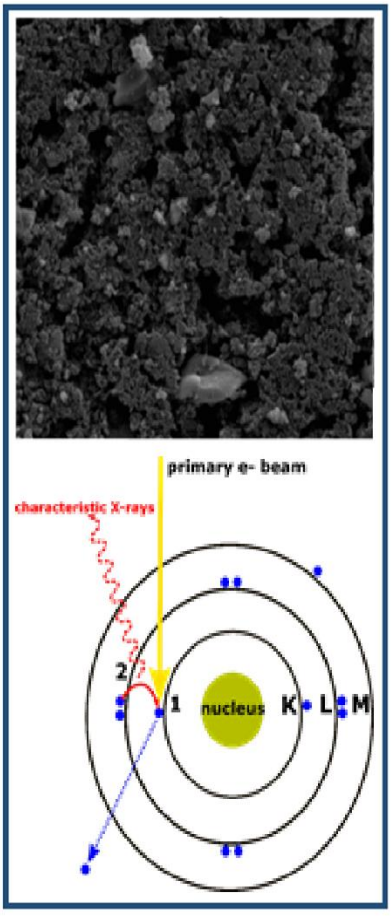


Figure 5. EDX micrograph of the $SiW_{11}Cd@CoFe_2O_4@PANI$ nanocomposite.

3.6. The ODS process results of gasoline/model fuels

Real gasoline contains mercaptans and other sulfur-containing compounds that need to be removed during the desulfurization process. ODS experiments using the synthesized nanocatalyst $SiW_{11}Cd@CoFe_2O_4@PANI$, were conducted to remove sulfur compounds from real gasoline and model fuel. Mercaptan removal was also investigated in detail. For the ODS process, 0.10 g of $SiW_{11}Cd@CoFe_2O_4@PANI$ was required, which was mixed with 50 mL of model fuel containing 500 ppmw DBT in n-heptane, and then 3 ml of H_2O_2/CH_3COOH was added using the experimental conditions specified in the experimental section. Table 1 shows the performance results of the synthesized nanocatalyst $SiW_{11}Cd@CoFe_2O_4@PANI$ in the ODS process of real fuel. The total sulfur content decreased by 96%, from 0.4988 wt.% to 0.0208 wt.%. Of course, this high percentage of total sulfur removal indicates the high catalytic activity of the *mono* substituted Keggin structure of the $SiW_{11}Cd$ compound in activating the H_2O_2 oxidant and converting resistant sulfur-containing aromatic compounds, such as DBT and its alkylated derivatives, to polar sulfoxides and sulfones that are easily extracted in the MeCN phase, which is a polar phase. It also removed 97% of the actual fuel mercaptans, which decreased from 98 ppm to 3 ppm. This significant reduction indicates the high efficiency of the ODS system using the nanocomposite $SiW_{11}Cd@CoFe_2O_4@PANI$ as a nanocatalyst in removing sulfur compounds. Comparison of fuel characteristics before and after the ODS process indicates that this nanocatalyst has a very effective performance in removing sulfur compounds, while other physical and qualitative characteristics of real gasoline have remained almost unchanged. For example, note that the density of gasoline at 15 °C has only changed from 0.7988 to 0.7986 g mL^{-1}, which is a very small difference and is considered within the experimental error range. This indicates that the desulfurization process does not cause significant destruction or modification of the main hydrocarbon components of the fuel

and exhibits good selectivity toward sulfur compounds. Also, the salt content of 17 ptb before and after the process remained constant, and the water content in gasoline was reported to be Nil in both cases. In summary, the results from Table 1 show that the $SiW_{11}Cd@CoFe_2O_4@PANI$ nanocatalyst under mild reaction conditions (1 hour and 35°C, using H_2O_2 as the oxidant) is capable of removing total sulfur and mercaptans from gasoline with very high efficiency, without significantly changing the physical properties and standard fuel specifications.

Table 1. The ODS results of real gasoline by $K_6SiW_{11}Cd@CoFe_2O_4@PANI$ nanocatalyst.

Entry	Properties of gasoline		Unit	ASTM Method	Before ODS	After ODS [a]
1	Total sulfur		wt.%	D 4294	0.4988	0.0208
2	Mercaptan		ppm	D 3227	98	3
3	Density		g/ml	D 1298	0.7988	0.7986
4	Salt		ptb	D 3230	17	17
5	Water content		vol.%	D 4006	Nil.	Nil.
6	Distillation	IBP	°C	D 86	49.7	49.4
		FBP			208.6	208.5
		10	vol.%		68.4	68.3
		50			119.3	119.2
		90			187.4	187.1
		95			207.4	207.2

[a] Condition of the ODS process: 0.10 g $K_6SiW_{11}Cd@CoFe_2O_4@PANI$, 50 mL of gasoline, 3 mL of H_2O_2-AcOH, 10 mL of CH_3CN solvent, reaction time = 1 h, and reaction temperature = 35 °C.

3.7. Effect of different types of catalysts on the desulfurization process

The effect of different types of catalysts on the desulfurization process was investigated using different catalysts, the results of which are shown in Table 2. Desulfurization was carried out without the presence of a catalyst, and the percentage of removal of Th, BT and DBT compounds was negligible, being 14%, 14% and 16%, respectively. These results indicate that the sulfur removal is mainly attributed to catalytic activity and not due to the oxidant or extraction. Since POMs can form active peroxo species, they have shown higher catalytic activity compared to the corresponding starting materials and base matrices, among which mono substituted polyoxometalates of $SiW_{11}Cd$ performed better, for example, $SiW_{11}Cd$ had the highest DBT removal efficiency. Among the catalysts reported in Table 2, the $SiW_{11}Cd@CoFe_2O_4@PANI$ was considered the most effective catalyst. This nanocatalyst was able to achieve desulfurization efficiencies of 96%, 96%, 97%, and 96% for Th, BT, DBT, and real gasoline, respectively, under mild reaction conditions (35 °C and 60 min) (Entry 1). These values are comparable to or higher than those reported for many advanced ODS catalysts [42]. Furthermore, among the various POM structures, the removal efficiency of sulfur compounds by Keggin structures is higher than that of Dawson structures [43]. The findings show that the immobilization of $SiW_{11}Cd$ on $CoFe_2O_4$ and PANI polymer matrix has shown a significant synergistic effect in the ODS process. Comparison of the individual catalyst components in Table 3 indicates the significant synergistic effect. The desulfurization efficiency relative to DBT increased from 27% for PANI, 53% for $CoFe_2O_4$, and 70% for $K_6SiW_{11}CdO_{39}$ to 97% for the ternary composite $SiW_{11}Cd@CoFe_2O_4@PANI$. This significant increase confirms the effective interaction between the active sites of the $SiW_{11}Cd$, the magnetic nanoparticles of $CoFe_2O_4$, and the PANI support, which leads to improved catalytic activity as well as accessibility to its active sites.

Table 2. Effect of different catalysts on the efficiency of the ODS process.

Entry	Catalyst	ODS efficiency (%)						
		Th	BT	DBT	Gasoline	Time (min)	Temperature (°C)	Ref.
1	$SiW_{11}Cd@CoFe_2O_4$ @PANI	96	96	97	96	60	35	This work
2	HPW/PIL	-	-	100	-	90	50	[41]
3	[Bmim]PW/HMS	-	79	98	-	90	60	[42]
4	$PMo_{12}/AmHMSiO_2$ @C	-	-	99	-	180	40	[43]
5	CTAB-PTA@CS	92	93	95	94	60	35	[44]
6	HPW/MWW	-	-	99.6	-	50	60	[45]
7	$K_3[PW_{12}O_{40}]$	58	59	60	58	60	35	[44]
8	$K_4[SiW_{12}O_{40}]$	56	56	58	55	60	35	[44]
9	$PMnW_{11}$	60	63	64	-	60	35	[31]
10	CuO	37	39	38	36	60	35	[46]
11	PANI	23	25	27	25	60	35	This work
12	$SiW_{11}Cd$	68	69	70	67	60	35	This work
13	$CoFe_2O_4$	48	50	53	47	60	35	This work
14	Without catalyst	14	14	16	13	60	35	This work

[a] Condition of the ODS process: 0.10 g $SiW_{11}Cd_9@CoFe_2O_4$@PANI, 50 mL model/real gasoline, 3 mL H_2O_2/CH_3COOH, 10 mL CH_3CN solvent, temperature = 35 °C, and time = 1 h.

The desulfurization efficiencies for Th, BT and DBT reached 96%, 96%, and 97%, respectively, at 1 h and 35 °C. As shown in Table 3, the electron density of the sulfur atom in BT, Th, and DBT, which are the sulfur-containing organic molecules in the fuel model we prepared, is given. Accordingly, it is clear that Th has the lowest electron density compared to other compounds. Therefore, it has the lowest reactivity in the desulfurization process and has the lowest removal percentage. For DBT, the highest electron density is seen and therefore has the highest reactivity and, consequently, the highest removal efficiency (Table 3).

Table 3. Electron density of the sulfur atom in compounds.

Compound	Electron density
Th	5.696
BT	5.739
DBT	5.758

3.8. Effect of different acid promoters on H_2O_2-based oxidative desulfurization

Desulfurization of gasoline and model fuels was carried out using the $SiW_{11}Cd@CoFe_2O_4@PANI$ nanocomposite in the presence of different acid promoters under otherwise identical reaction conditions, and the results are summarized in Table 4. The H_2O_2 concentration and acid loading were kept constant in all experiments, corresponding to a fixed 2:1, (v/v). The catalyst loading, fuel volume, reaction temperature, reaction time, and extraction conditions were also maintained constant. Therefore, the differences in desulfurization efficiency can primarily be attributed to the nature of the acid promoter rather than variations in the amounts of H_2O_2 or acid. Among the acid promoters investigated, the H_2O_2/acetic acid system exhibited the highest ODS performance, with sulfur removal efficiencies of 96%, 96%, 97%, and 96% for Th, BT, DBT, and real gasoline, respectively. The superior performance of acetic acid in the presence of H_2O_2 can be attributed to the formation of peracetic acid (CH_3COOOH), a reactive oxidizing species capable of promoting the oxidation of sulfur compounds. When benzoic acid (C_6H_5COOH) was used instead of acetic acid, the ODS efficiency decreased, with sulfur removal ranging from 88% to 91%.

The use of oxalic acid resulted in a further decrease in sulfur removal. The lowest ODS efficiencies were observed for sulfuric acid and carbonic acid. These results indicate that acid strength alone does not determine ODS performance; rather, the nature of the acid promoter and its ability to participate effectively in the formation of reactive oxidizing species are important factors governing the efficiency of the H_2O_2-based ODS process

Table 4. Effect of different acid promoters on H_2O_2-based oxidative desulfurization**.**

Entry	Oxidant	ODS efficiency (%)			
		DBT	BT	Th	Gasoline
1	CH_3COOH	97	96	96	96
2	C_6H_5COOH	91	91	90	88
3	HO−C(=O)−C(=O)−OH	87	86	85	85
4	Sulfuric acid	71	70	69	67
5	Carbonic acid	70	68	67	67

3.9. Effect of dosage of nanocatalyst on the ODS process

The amount of catalyst certainly has an effect on the ODS process of model fuel and gasoline. In order to determine the extent of the effect, different amounts of the synthesized nanocomposite ($SiW_{11}Cd@CoFe_2O_4@PANI$) ranging from 0 to 0.11 g were used in the ODS process. The experimental results are shown in Figure 6.

The results show that the amount of $SiW_{11}Cd@CoFe_2O_4@PANI$ is one of the key and effective parameters in the ODS process. By increasing the amount of $SiW_{11}Cd@CoFe_2O_4@PANI$, the number of available active sites and the concentration of reactive peroxo species increase, and as a result, the sulfur removal efficiency increases. In other words, by increasing the dose of $SiW_{11}Cd@CoFe_2O_4@PANI$ to a certain amount, the performance of the ODS process increases significantly. However, the results showed that increasing the catalyst amount from 0.10 to 0.11 g did not have a significant effect on the sulfur removal efficiency and the reaction efficiency of the process remained almost constant.

This behavior can be attributed to the excessive accumulation of peroxide species and the creation of mass transfer limitations and steric barriers in the reaction medium, which prevent the access of sulfur compounds to the active sites of $SiW_{11}Cd@CoFe_2O_4@PANI$ and consequently the oxidation of sulfur compounds. Therefore, according to the results obtained, the amount of 0.10 g was selected as the optimal amount of $SiW_{11}Cd@CoFe_2O_4@PANI$ to achieve the highest sulfur removal efficiency.

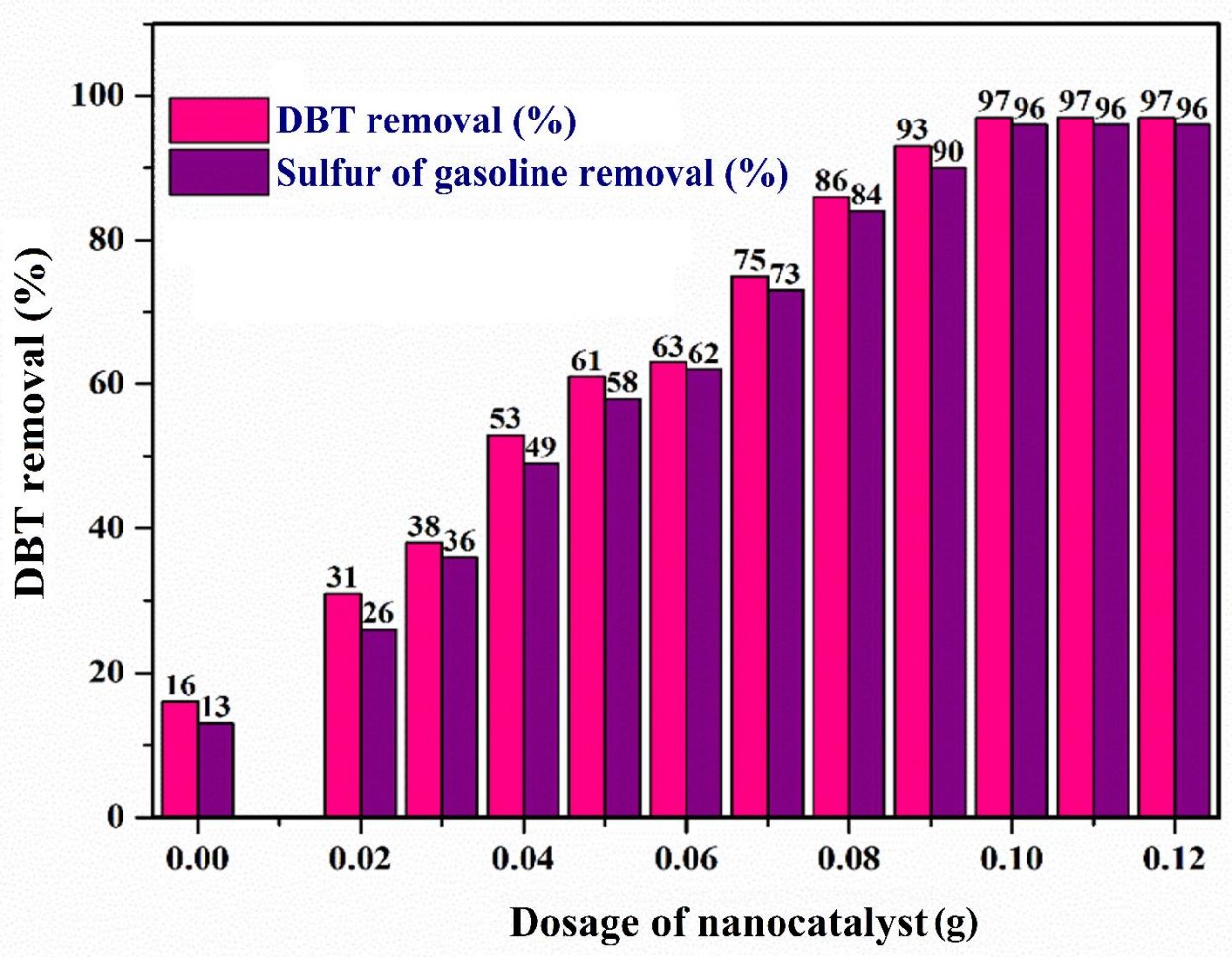


Figure 6. Effect of $SiW_{11}Cd@CoFe_2O_4@PANI$ amount on ODS of DBT and gasoline.

3.10. Effect of time and temperature on the ODS process

In order to investigate the effect of time and temperature on the ODS process of DBT and real gasoline, several experiments were conducted using the synthesized catalysts $SiW_{11}Cd@CoFe_2O_4@PANI$. These experiments were conducted for 0 to 60 minutes and in the temperature range of 25 to 40 °C. The results showed that the sulfur removal efficiency increases with increasing ODS reaction time. The reactions reached equilibrium after 60 minutes. After 1 h, the active sites of the catalyst became increasingly saturated due to the sulfur molecules present and the sulfoxides and sulfones produced by the reaction, which causes the activity of the sites available for oxidation to decrease and, consequently, the efficiency of the ODS process does not increase. As shown in Figure 7, the slope of the graph is high in the first 10 or 20 minutes of the reaction, which is due to the high number of active sites of the catalyst and the high concentration of DBT. Consequently, the reaction rate is initially high. As the reaction proceeds, the active sites of $SiW_{11}Cd@CoFe_2O_4@PANI$ are occupied and the DBT concentration decreases, so the curve goes to a steady state. The catalytic activity of the $SiW_{11}Cd@CoFe_2O_4@PANI$ nanocomposite was initially demonstrated by desulfurization efficiencies exceeding 70% for both DBT and real gasoline after 1 h at 25 °C. Further optimization of the reaction parameters indicated that increasing the reaction temperature to 35-40 °C significantly improved the oxidative desulfurization performance. Based on the experimental findings, 35 °C and a reaction time of 1 h were selected as the optimum operating conditions, providing an appropriate balance between desulfurization efficiency and mild processing conditions [45,46].

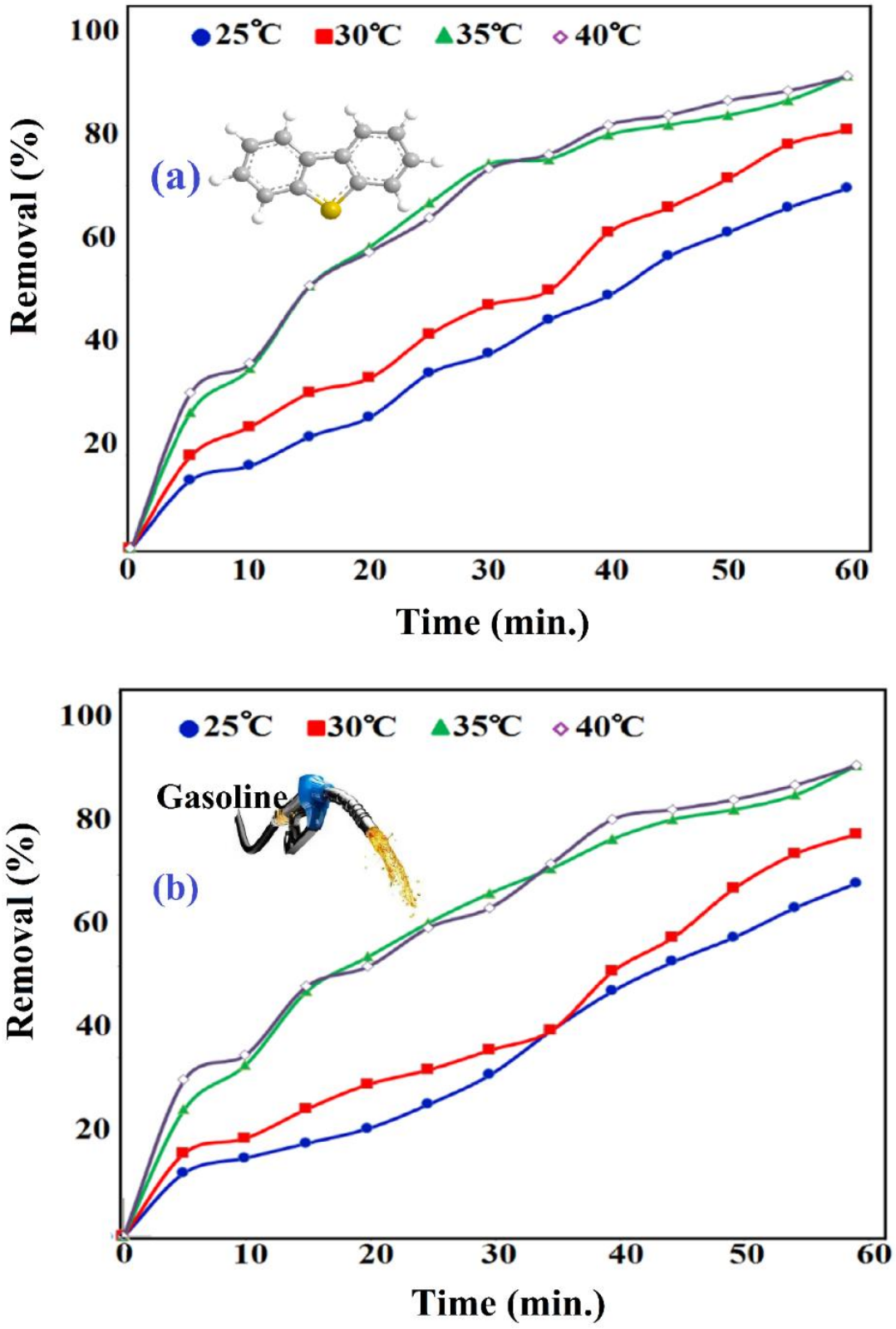


Figure 7. Effect of time and temperature on the ODS process of (a) DBT and (b) gasoline.

3.11. Recyclability performance of nanocatalyst

The recyclability of the $SiW_{11}Cd@CoFe_2O_4@PANI$ nanocatalyst was evaluated over five consecutive catalytic cycles under the optimized reaction conditions. After each reaction cycle, the catalyst was readily separated from the reaction mixture using an external magnet owing to the magnetic properties of the $CoFe_2O_4$ component. The recovered catalyst was subsequently washed, dried, and reused in the next catalytic cycle under identical reaction conditions. As shown in Figure 8a, the XRD patterns of the fresh catalyst and the recovered catalyst after the first, third, and fifth cycles were highly similar. No significant changes in the characteristic diffraction peaks or the appearance of additional crystalline phases were observed after repeated use. These results indicate that the main crystalline structure of the $SiW_{11}Cd@CoFe_2O_4@PANI$ nanocatalyst was retained during the recycling process. The catalytic performance of the recovered catalyst was also evaluated for the oxidative desulfurization of DBT (Figure 8b). The catalyst maintained a high sulfur-removal efficiency over five consecutive cycles. After the fifth cycle, the DBT removal efficiency decreased slightly to approximately 95%, compared with the higher efficiency obtained with the fresh catalyst. This relatively small decrease indicates that the nanocatalyst retains most of its catalytic activity after repeated use. The observed decrease in catalytic performance after repeated cycles may be associated with partial blockage or occupation of accessible active sites by adsorbed sulfur-containing species formed during the oxidation process [18,20,44]. However, this interpretation requires further post-reaction characterization to be confirmed. In addition, although the preservation of the XRD pattern demonstrates structural stability, it does not by itself establish the absence of leaching of the polyoxometalate or metal species. Therefore, further analyses, such as ICP-OES or ICP-MS of the reaction solution, would be useful to quantitatively evaluate possible leaching during repeated catalytic cycles. Overall, the combination of magnetic separability and

the retention of high catalytic activity over five consecutive cycles demonstrates the good reusability of the $SiW_{11}Cd@CoFe_2O_4@PANI$ nanocatalyst and highlights its potential as a recyclable heterogeneous catalyst for oxidative desulfurization.

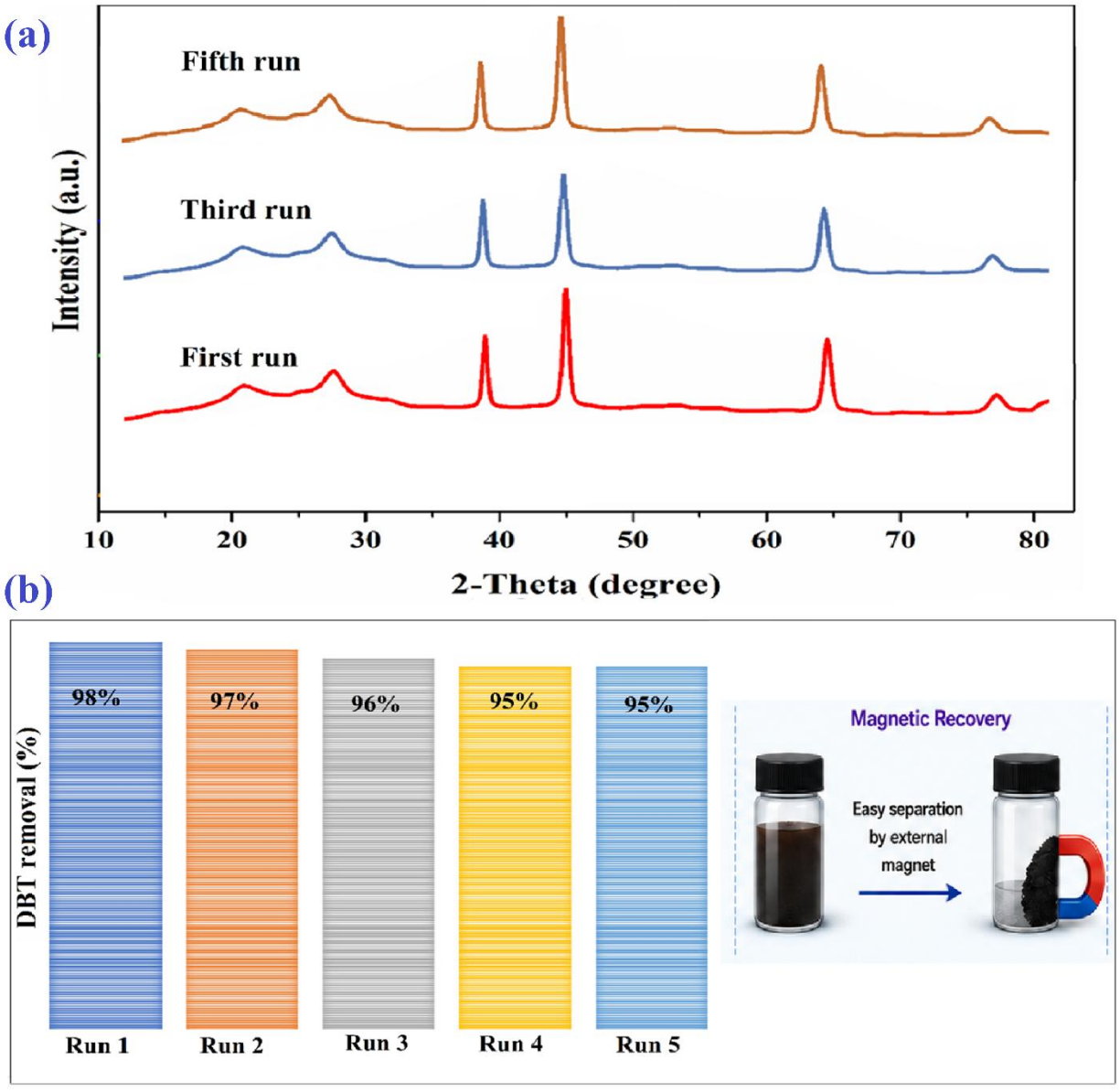


Figure 8. XRD pattern of (a) fresh $SiW_{11}Cd@CoFe_2O_4@PANI$, (b) after first, (c) third, and (d) fifth run reuse and recyclability performance of nanocatalyst in the ODS of DBT.

3.12. Kinetics of gasoline and DBT oxidation reaction

To better understand the reaction mechanism of the catalytic oxidation of sulfur-containing aromatic compounds, a kinetic study was performed. The oxidative conversion of these sulfur-containing aromatic species was investigated over a 1-hour reaction time in the temperature range of 25–40 °C. Using a first-order kinetic model (Eq. 3), the rate constant k was determined using the following equation:

$$-\frac{dC}{dt} = kC \tag{3}$$

$$\int_{C_o}^{C} \frac{dC}{C} = \ln\frac{C}{C_o} = -kt \tag{4}$$

$$C = C_o e^{-kt} \tag{5}$$

Where:

$$k = Ae^{\frac{-E_a}{RT}} \tag{6}$$

the apparent rate constants for gasoline and DBT oxidation was determined using their initial concentrations (Co) and concentrations at time t (Ct) in the $\ln(C/C_0)$ or C/C_0 versus t plot (Eq. 5). As can be seen in Figure 9, the C/C_0 concentration ratio decreases continuously with increasing time at all temperatures studied, indicating the progress of the reaction and the removal of DBT from the reaction medium. Increasing the temperature from 25 to 40 °C caused a significant increase in the C/C_0 reduction rate in both DBT and gasoline systems. This effect was more pronounced at temperatures of 35 and 40 °C, and at long times, the DBT concentration reached very low values. A comparison of the two systems shows that although the presence of the gasoline

matrix causes a slight change in the kinetic process, the positive effect of increasing temperature on DBT removal is still maintained. The C/C_0 reduction trend with time is also qualitatively consistent with a pseudo-first-order kinetic behavior. Therefore, increasing temperature is an effective factor in improving the DBT removal rate, and the resulting data can be used to determine the apparent rate constant and activation energy of the process. The resulting regression parameters are summarized in Table 5. The temperature dependence of the reaction rate constant (k) was evaluated using the Arrhenius equation (Eq. (6)). A is the pre-exponential factor, Ea is the apparent activation energy, R and T are the gas constant and reaction temperature (K), respectively [44]. Linear regression of the Arrhenius plots (Figure 10) yielded apparent activation energies of 53.25 kJ/mol for the DBT model fuel and 49.78 kJ/mol for the gasoline sample.

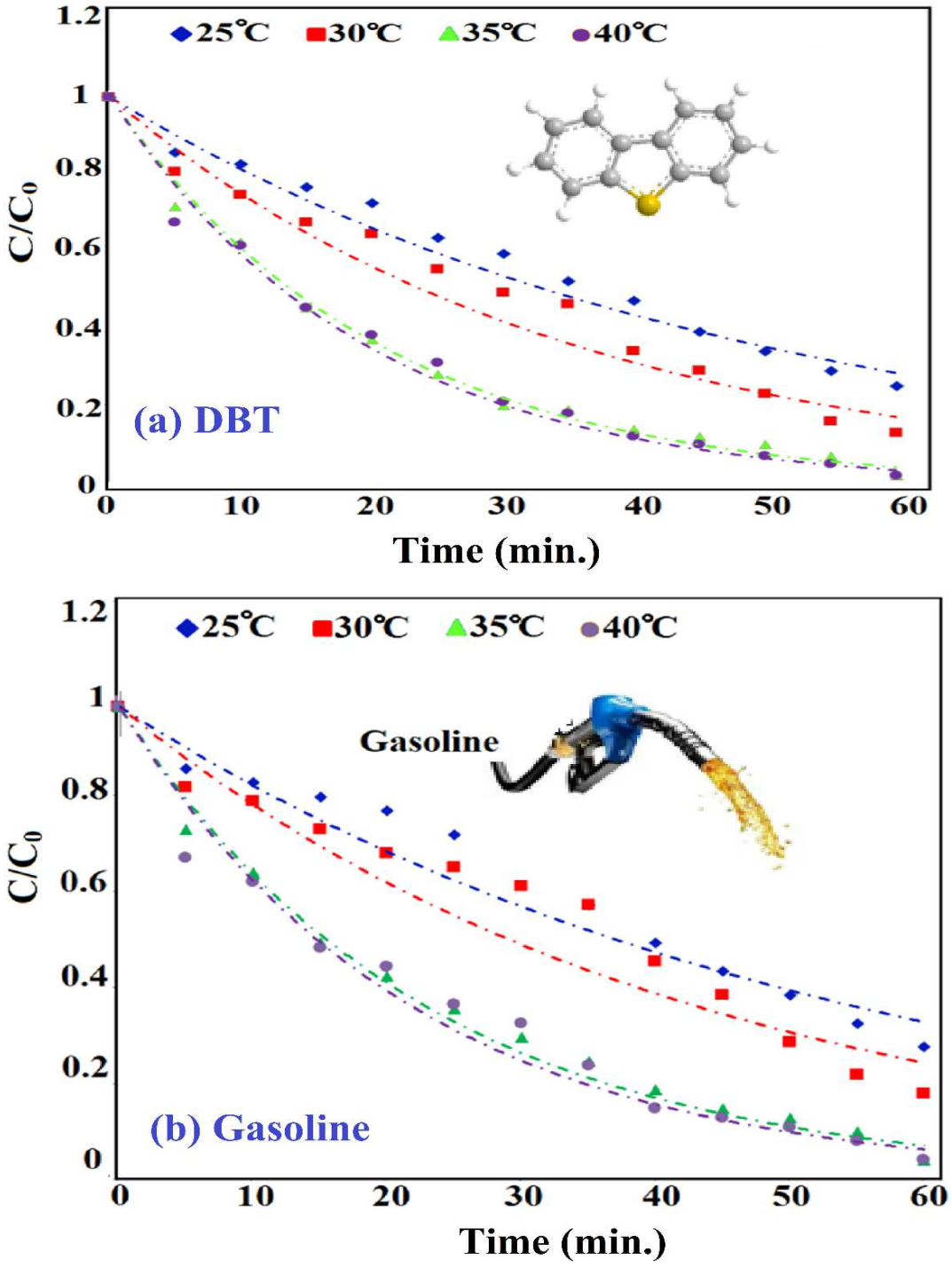


Figure 9. Plots of C/C_0 for the oxidation of a) DBT and b) gasoline.

Table 5. Pseudo-first-order rate constants and correlation factors of the DBT and gasoline.

Temperature (°C)	Rate constant k (min^{-1})		Correlation factor R^2	
	DBT	Gasoline	DBT	Gasoline
25	0.02	0.021	0.9712	0.9187
30	0.028	0.025	0.9445	0.8892
35	0.049	0.041	0.9596	0.9174
40	0.052	0.050	0.9805	0.9477

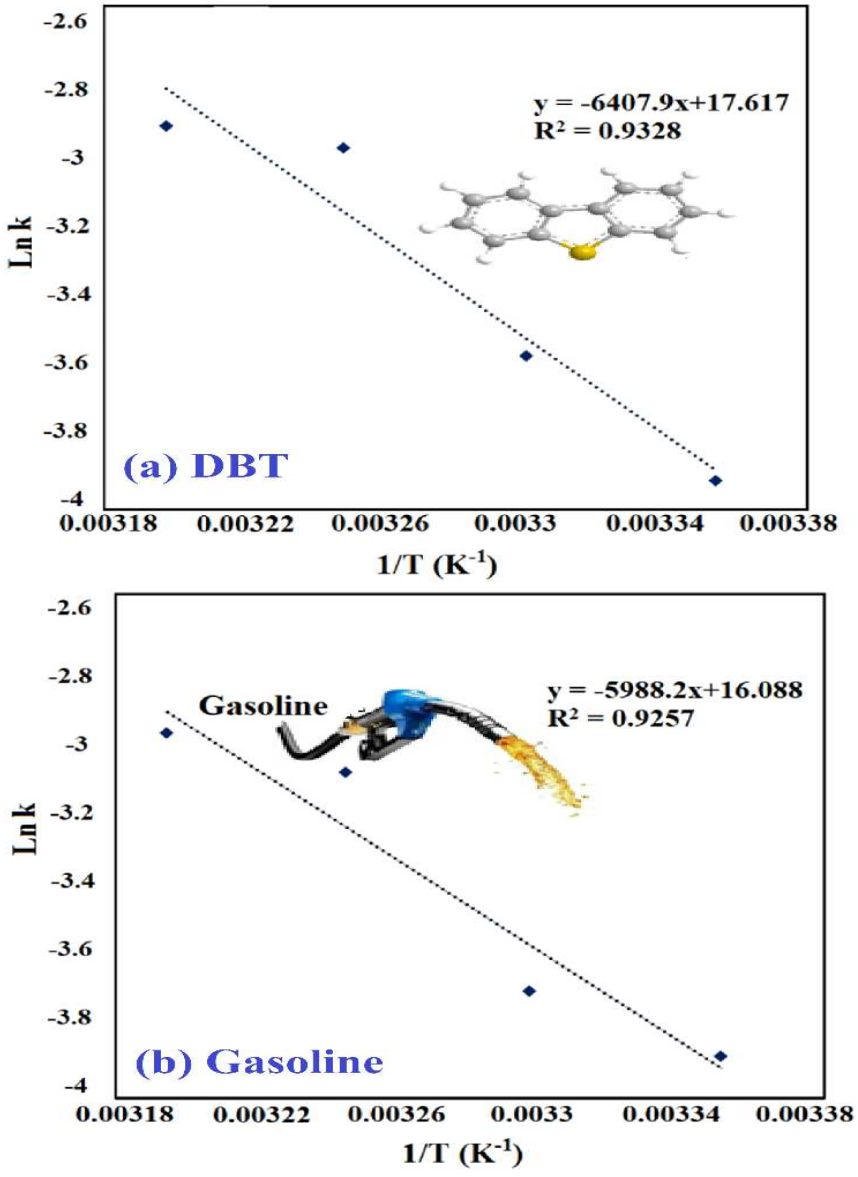
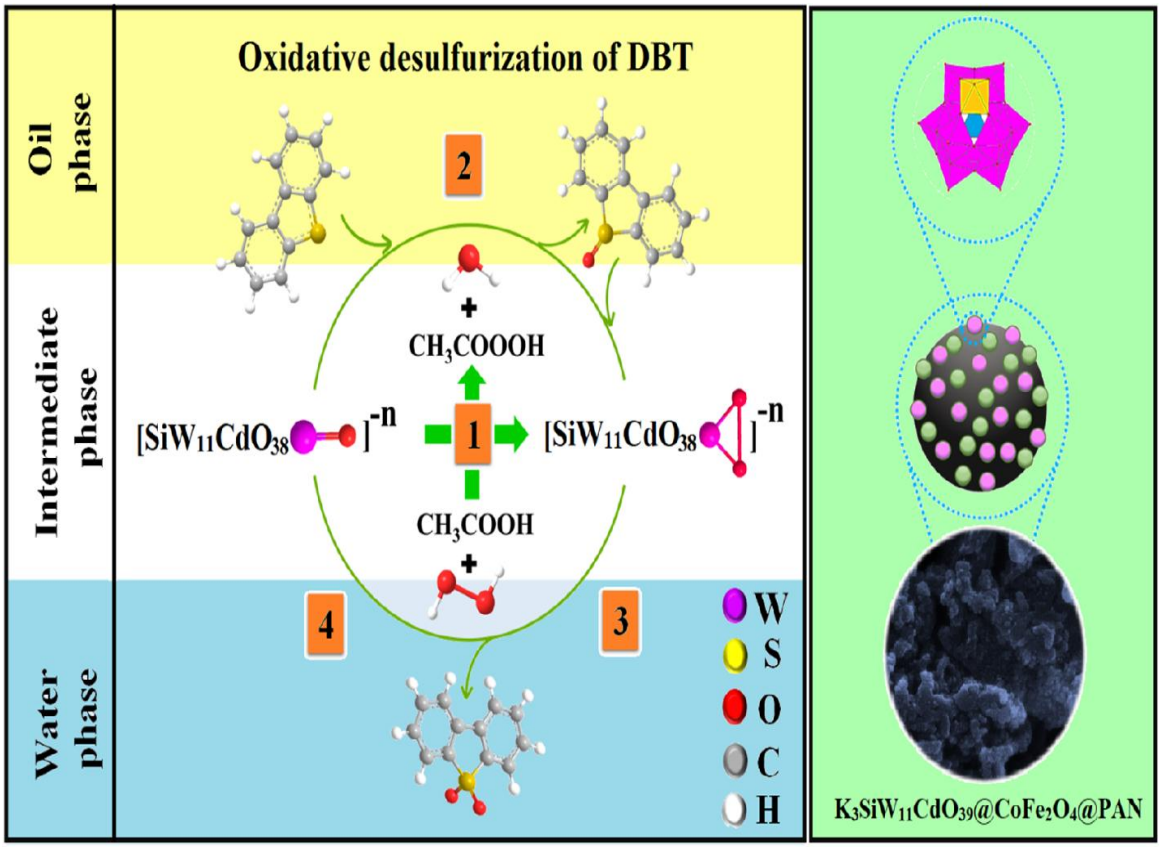


Figure 10. Arrhenius plot for the oxidation of (a) DBT and (b) gasoline.

3.13. Proposed mechanism of the ODS process

A possible mechanism for the ODS process catalyzed by $SiW_{11}Cd@CoFe_2O_4@PANI$ nanocatalyst is proposed as follows: Before ODS occurs, DBT is in the nonpolar oil phase. When the $SiW_{11}Cd@CoFe_2O_4@PANI$ and H_2O_2/CH_3COOH are added, the oxidation reactions occur mainly at the interface between the oil and aqueous phases (intermediate phase). The formation of the peroxo-tungstate intermediate complex ($W(O)_2$), shown in Scheme 1, facilitates the elucidation of the oxidation mechanism of sulfur-containing compounds, as this intermediate acts as an important intermediate in polyoxometal-catalyzed oxidation reactions (Scheme 1). A mixture of H_2O_2/CH_3COOH is used to form the peracetic acid intermediate (CH_3COOOH). By producing CH_3COOOH, which is a good intermediate as a source of active oxygen, the terminal tungstate atoms (W=O) accept active oxygen from the CH_3COOOH, and then the electrophilic complex $W(O)_2$ is formed in the intermediate phase (step 1). The by-products of this oxidation reaction are water molecules. According to previously published papers, the oxidation of DBT occurs via an electrophilic mechanism [18,20,44]. By electrophilic attack of the complex ($W(O)_2$) on the sulfur atom, DBT is converted to the corresponding sulfoxides (DBTO) or sulfones ($DBTO_2$) (steps 2 and 3). After the oxidation process occurs, the reaction products are collected in the aqueous phase due to their polar nature, which can be considered as an advantage for the final step, which is extraction with MeCN solvent (Step 4). The high polarity of MeCN makes it a suitable option to increase the polarity of the aqueous phase in order to improve the extraction of polar sulfur compounds. Also, $CoFe_2O_4$ nanoparticles may promote the decomposition of H_2O_2, potentially generating reactive oxygen species such as •OH radicals. These generated radicals can further accelerate the oxidation of DBT and improve the overall efficiency of DBT ODS. The close contact between $CoFe_2O_4$ and $SiW_{11}Cd$ may facilitate rapid electron transfer. The role of PANI in the

catalytic system is manifold. Due to its conjugated π-electron network, it provides mechanical stability and prevents aggregation of $CoFe_2O_4$ nanoparticles and $SiW_{11}Cd$ clusters. These factors may facilitate interfacial electron transport and facilitate continuous oxidation-reduction cycling of the catalytic centers. A porous polymer matrix improves DBT adsorption through π-π interactions and increases the local concentration of DBT around the active sites. The excellent catalytic performance of the $SiW_{11}Cd@CoFe_2O_4@PANI$ can be attributed to the synergistic interaction between the $SiW_{11}Cd$ active centers, the magnetic $CoFe_2O_4$, and the conductive PANI. The combination of efficient oxygen transport, increased accessibility to active sites, and improved DBT adsorption leads to enhanced ODS efficiency of DBT.



Scheme. 1. Proposed ODS mechanism of DBT by $SiW_{11}Cd@CoFe_2O_4@PANI$.

4. CONCLUSION

In this study, a recyclable hybrid nanocatalyst, $SiW_{11}Cd@CoFe_2O_4@PANI$, was prepared and evaluated for the ODS of model sulfur compounds and real gasoline. The structural and morphological characterization results confirmed the incorporation of the POM and $CoFe_2O_4$ components within the polyaniline-based composite. The catalytic results demonstrated that the hybrid catalyst exhibited substantially higher sulfur-removal activity than the individual components, suggesting a beneficial contribution from the combination of the POM, $CoFe_2O_4$, and PANI components. Under the optimized reaction conditions, the catalyst achieved high removal efficiencies for DBT, Th, and BT, while efficient sulfur removal was also obtained from real gasoline. In particular, the total sulfur content of the gasoline decreased from 0.4988 wt% (4988 ppm) to 0.0208 wt% (208 ppm), corresponding to approximately 96% sulfur removal. Mercaptan sulfur was reduced from 98 to 3 ppm, corresponding to approximately 97% removal. The high activity obtained under relatively mild reaction conditions demonstrates the potential of the prepared hybrid material for ODS of fuel. Kinetic studies indicated that the oxidation process could be described by a pseudo first order model within the investigated temperature range. The calculated activation energies were 53.25 kJ mol^{-1} for DBT oxidation and 49.78 kJ mol^{-1} for sulfur removal from gasoline. Furthermore, the catalyst retained a substantial portion of its catalytic activity after five consecutive reaction cycles, while XRD analysis indicated that its main structural features were maintained after reuse. Based on the experimental results, the enhanced ODS performance is proposed to arise from the combined contributions of the polyoxometalate and $CoFe_2O_4$ active components, together with the adsorption and support properties of PANI. A possible reaction pathway involves activation of H_2O_2 and subsequent oxidation of sulfur containing compounds to their corresponding sulfoxides and sulfones, followed by their

preferential removal during the extraction step. However, further studies, including direct analysis of metal/POM leaching and radical-species identification, are required to establish the detailed reaction mechanism and the origin of the enhanced catalytic activity. Overall, the $SiW_{11}Cd@CoFe_2O_4@PANI$ hybrid catalyst shows promise as a reusable catalyst for the ODS of real gasoline. Its high sulfur removal efficiency, relatively mild operating conditions, and recyclability make this composite a potentially attractive candidate for further development of practical deep desulfurization processes.

DECLARATIONS

Acknowledgements

The authors would like to thank University of Zanjan for providing the laboratory facilities and technical support required to conduct this research.

Funding

The authors declare that no funds, grants, or other financial support were received during the preparation of this study.

Authors' Contributions

All authors contributed to the conception and design of the study. Material preparation, experiments, data collection, and analysis were performed by the authors. The first draft of the manuscript was written by the first author, and all authors reviewed, revised, and approved the final version of the manuscript.

Ethical Approval

Not applicable.

Consent to Participate

Not applicable.

Consent to Publish

Not applicable.

Competing Interests

The authors declare that they have no known competing financial interests or personal relationships that could have appeared to influence the work reported in this paper.

Data Availability Statement

The datasets generated and/or analyzed during the current study are available from the corresponding author upon reasonable request.

REFERENCES

(1) Sachdeva, T. O.; PANIt, K. K. Deep desulfurization of diesel via peroxide oxidation using phosphotungstic acid as phase transfer catalyst. *Fuel Process. Technol.* **2010**, *91*, 1133–1138.

(2) Rezvani, M. A.; Oveisi, M.; Alinia Asli, M. Phosphotungestovanadate immobilized on PVA as an efficient andreusable nano catalyst for oxidative desulfurization of gasoline. *J. Mol. Catal. A: Chem*. **2015**, *410*, 121–132.

(3) Chen, Y.; Wang, S.; Xue, L.; Zhang, Z.; Li, H.; Wu, L.; Wang, Y.; Li, F.; Zhang, F.; Li, Y. Insights into the working mechanism of cathode interlayers in polymer solar cells via $[(C_8H_{17})_4N]_4[SiW_{12}O_{40}]$. *J. Mater. Chem. A* **2016**, *4*, 19189–19196.

(4) Leng, Y.; Zhao, J.; Jiang, P.; Wang, J. Amphiphilic polyoxometalate-paired polymer coated Fe_3O_4: Magnetically recyclable catalyst for epoxidation of bio-derived olefins with H_2O_2. *ACS Appl. Mater. Interfaces* **2014**, *6*, 5947–5954.

(5) Leng, Y.; Wu, J.; Jiang, P.; Wang, J. Amphiphilic phosphotungstate-paired ionic copolymer as a highly efficient catalyst for triphase epoxidation of alkenes with H_2O_2. *Catal. Sci. Technol*. **2014**, *4*, 1293–1300.

(6) Wang, S. S.; Yang, G. Y. Recent Advances in Polyoxometalate-Catalyzed Reactions. *Chem. Rev.* **2015**, *115*, 4893–4962.

(7) Izzet, G.; Ishow, E.; Delaire, J.; Afonso, C.; Tabet, J. C.; Proust, A. Photochemical activation of an azido manganese-monosubstituted Keggin polyoxometalate: On the road to a Mn(V)−nitrido derivative. *Inorg. Chem.* **2009**, *48*, 11865–11870.

(8) Estrada, A. C.; Santos, I. C. M. S.; Simões, M. M. Q.; Neves, M. G. P. M. S.; Cavaleiro, J. A. S.; Cavaleiro, A. M. V. Silica supported transition metal substituted polyoxotungstates: Novel heterogeneous catalysts in oxidative transformations with hydrogen peroxide. *App. Catal. A: Gen*. **2011**, *392*, 28–35.

(9) Pathan, S.; Patel, A. Keggin type transition metal substituted phosphomolybdates: heterogeneous catalysts for selective aerobic oxidation of alcohols and alkenes under solvent free condition. *Catal. Sci. Technol.* **2014**, *4*, 648–656.

(10) Rezvani, M. A.; Fallah Shojaie, A.; Loghmani, M. H. Synthesis and characterization of novel nanocomposite, anatase sandwich type polyoxometalate, as a reusable and green nano catalyst in oxidation desulfurization of simulated gas oil. *Catal. Commun*. **2012**, *25*, 36–40.

(11) Li, K.; Wang, J.; Zou, Y.; Song, X.; Gao, H.; Zhu, W.; Zhang, W.; Yu, J.; Jia, M. Surfactant-assisted sol–gel synthesis of zirconia supported phosphotungstates or Ti-substituted phosphotungstates for catalytic oxidation of cyclohexene. *App. Catal. A: Gen*. **2014**, *482*, 84–91.

(12) North, J.; Poole, O.; Alotaibi, A.; Bayahia, H.; Kozhevnikova, E. F.; Alsalme, A.; Siddiqui, M. R. H.; Kozhevnikov, I. V. Efficient hydrodesulfurization catalysts based on Keggin polyoxometalates. *App. Catal. A: Gen*. **2015**, *508*, 16–24.

(13) Borhade, A. V.; Uphade, B. K.; Tope, D. R. PbO as an efficient and reusable catalyst for one-pot synthesis of tetrahydro benzo pyrans and benzylidene malonitriles. *J. Chem. Sci*. **2013**, *125*, 583–589.

(14) Allen, G. C.; Paul, M. Catalytic effect of vanadium, iron and lead oxides on the oxidation of moderator graphite. *J. Chem. Soc. Faraday Trans*. **1995**, *91*, 3717–3723.

(15) Fallah Shojaei, A.; Rezvani, M. A.; Loghmani, M. H. Comparative study on oxidation desulfurization of real gas oil and model sulfur compounds with hydrogen peroxide promoted by formic acid: Synthesis and characterization of vanadium containing polyoxometalate supported on anatase crushed nanoleaf. *Fuel Process. Technol*. **2014**, *118*, 1–6.

(16) Ghaedi, M.; Ghaedi, A. M.; Mirtamizdoust, B.; Agarwal, S.; Kumar Gupta, V. Simple and facile sonochemical synthesis of lead oxide nanoparticles loaded activated carbon and its application for methyl orange removal from aqueous phase. *J. Mol. Liq*. **2016**, *213*, 48–57.

(17) Rezvani, M. A.; Fallah Shojaei, A.; Mohamadi Zonoz, F. Anatase titania–vanadium polyphosphomolybdate as an efficient and reusable nano catalyst for the desulfurization of gas oil. *J. Serb. Chem. Soc*. **2014**, *79*, 1099–1110.

(18) Rezvani, M. A.; Alinia Asli, M.; Oveisi, M.; babaei, R.; Qasemi, K.; Khandan, S. An organic-inorganic hybrid based on Anderson-type polyoxometalate immobilized on PVA as a reusable and efficient nanocatalyst for oxidative desulfurization of gasoline. *RSC Adv*. **2016**, *6*, 53069–53079.

(19) Rezvani, M. A.; Alinia Asli, M.; Khandan, S.; Mousavi, H.; Shokri Aghbolagh, Z. Synthesis and characterization of new nanocomposite CTAB-PTA@CS as an efficient heterogeneous catalyst for oxidative desulfurization of gasoline. *Chem. Eng. J.* **2017**, *312*, 243–251.

(20) Arulmozhi, K. T.; Mythili, N. Studies on the chemical synthesis and characterization of lead oxide nanoparticles with different organic capping agents. *AIP Adv*. **2013**, *3*, 122122–122131.

(21) Abdalla, Z. E. A.; Li, B. Preparation of MCM-41 supported $(Bu_4N)_4H_3(PW_{11}O_{39})$ catalyst and its performance in oxidative desulfurization. *Chem. Eng. J*. **2012**, *200–202*, 113–121.

(22) Rezvani M. A., Ardeshiri H. H., Aghasadeghi Z.; Extractive–Oxidative Desulfurization of Real and Model Gasoline Using $(gly)_3H[SiW_{12}O_{40}]\subset CoFe_2O_4$ as a Recoverable and Efficient Nanocatalyst. *Energy Fuels*. **2023**; 37 (3): 2245–2254.

https://doi.org/10.1021/acs.energyfuels.2c03265

(23) Satyaranjan B.; A Review on Polyaniline-Supported Catalyst for Organic Transformations. *ACS Omega* **2024,** 9 (51): 50097–50117. https://doi.org/10.1021/acsomega.4c04352.

(24) Sunil K. Pillalamarri, Frank D. Blum, Akira T. Tokuhiro, Massimo F. Bertino; One-Pot Synthesis of Polyaniline−Metal Nanocomposites. *Chem. Mater*. **2005**; 17 (24): 5941–5944. https://doi.org/10.1021/cm050827y

(25) Chamack, M.; Mahjoub, A. R.; Aghayan, H. Cesium salts of tungsten-substituted molybdophosphoric acid immobilized onto platelet mesoporous silica: Efficient catalysts for oxidative desulfurization of dibenzothiophene. *Chem. Eng. J*. **2014**, *255*, 686–694.

(26) Qiu, J.; Wang, G.; Zeng, D.; Tang, Y.; Wang, M.; Li, Y. Oxidative desulfurization of diesel fuel using amphiphilic quaternary ammonium phosphomolybdate catalysts. *Fuel Process. Technol*. **2009**, *90*, 1538–1542.

(27) Rezvani M.A.; Bakhtiari A.; Rahmani P. Synthesis and characterization of new nanocomposite PW11Mn@CuO@PAN as an efficient nanocatalyst for deep oxidative desulfurization of real/model fuels, *Mater. Sci. Eng. B* **2024**, 303, 117314.

(28) Li, D.; Ma, P.; Niu, J.; Wang, J. Recent advances in transition-metal-containing Keggin-type polyoxometalate-based coordination polymers. *Coord. Chem. Rev*. **2019**, 392, 49-80.

(29) Lü, H.; Deng, C.; Ren, W.; Yang, X. Oxidative desulfurization of model diesel using $[(C_4H_9)_4N]_6Mo_7O_{24}$ as a catalyst in ionic liquids. *Fuel Process. Technol*. **2014**, *119*, 87–91.

(30) Rezvani M. A., Shaterian M., Shokri A. Z., Akbarzadeh F., Synthesis and characterization of new nanocomposite CTAB@POM@TiO_2 as an efficient heterogeneous catalyst for oxidative desulfurization of gas oil, *Nano-Micro Chem*. **2018**, 49, 23-32.

(31) Rezvani, M. A.; Hosseini, S.; Hassani A. H. Highly Efficient Catalytic Oxidative Desulfurization of Gasoline Using $PMnW_{11}$@PANII@CS as a New Inorganic–Organic Hybrid Nanocatalyst. *Energy Fuels*. **2022**, 36, 7722-7732.

(32) Zou, J.; Lin, Y.; Yang, C. Covalency triggers high catalytic activity of amorphous molybdenum oxides for oxidative desulfurization. *Sci. China Chem*. **2023**, *66*, 1211-1220.

(33) Zou, J.; Lin, Y.; Wu, S.; Zhong, Y.; Yang, C. Molybdenum dioxide nanoparticles anchored on nitrogen-doped carbon nanotubes as oxidative desulfurization catalysts: role of electron transfer in activity and reusability. *Adv. Funct. Mater*. **2021**, *31*, 2100442.

(34) Cychosz, K. A.; Wong-Foy, A. G.; Matzger, A. J. Enabling cleaner fuels: desulfurization by adsorption to microporous coordination polymers. *J. Am. Chem. Soc*. **2009**, 131, 14538-14543.

(35) Xu, J.; Zhao, S.; Chen, W.; Wang, M.; Song, Y. F. Highly efficient extraction and oxidative desulfurization system using $Na_7H_2LaW_{10}O_{36}\cdot 32H2O$ in [bmim]BF_4 at room temperature. *Chem. Eur. J*. **2012**, 18, 4775-4781.

(36) Xu, J.; Zhang, B.; Lu, Y.; Wang, L.; Tao, W.; Teng, X.; Zhang, Z. Adsorption desulfurization performance of PdO/SiO_2@ graphene oxide hybrid aerogel: Influence of graphene oxide. *J. Hazard. Mater*. **2022**, 421, 126680.

(37) Cape, J. N.; Fowler, D.; Davison, A. Ecological effects of sulfur dioxide, fluorides, and minor air pollutants: recent trends and research needs. *Environ. Int*. **2003**, 29, 201-211.

(38) Zhou, W.; Zhou, A.; Zhang, Y.; Zhang, C.; Chen, Z.; Liu, L.; Tao, X. Hydrodesulfurization of 4, 6-dimethyldibenzothiophene over NiMo supported on Ga-modified Y zeolites catalysts. *J. Catal*. **2019**, 374, 345-359.

(39) Martínez, I.; Mohamed, M. E. S.; Santos, V. E.; García, J. L.; García-Ochoa, F.; Díaz, E.. Metabolic and process engineering for biodesulfurization in Gram-negative bacteria. *J. Biotechnol*. **2017**, 262, 47-55.

(40) Li, C.; Zhang, J.; Li, Z.; Yin, J.; Cui, Y.; Liu, Y.; Yang, G. Extraction desulfurization of fuels with 'metal ions' based deep eutectic solvents (MDESs). *Green Chem*. **2016**, 18, 3789-3795.

(41) Flores, R., Rodas, A. Gasperin, R. Oxidative desulfurization of diesel fuel oil using supported Fenton catalysts and assisted with ultrasonic energy. *Pet. Sci.* **2019**, 16, 1176–1184. https://doi.org/10.1007/s12182-019-0349-z

(42) Tang, L., Luo, G., Kang, L. et al. A novel [Bmim]PW/HMS catalyst with high catalytic performance for the oxidative desulfurization process. *Korean J. Chem. Eng.* **2013**, 30, 314–320 (2013). https://doi.org/10.1007/s11814-012-0182-1

(43) Zhang, R.; Ding, H.; Pu, X.; Qian, Z.; Xiao, Y. Recent Advances in the Synthesis of Sulfides, Sulfoxides and Sulfones via C-S Bond Construction from Non-Halide Substrates. *Catalysts* **2020**, *10*, 1339. https://doi.org/10.3390/catal10111339

(44) Rezvani M. A., Khalafi N., Deep oxidative desulfurization of real fuel and thiophenic model fuels using polyoxometalate-based catalytic nanohybrid material, *Materials Today Communications*, **2020**, 22, 100730. https://doi.org/10.1016/j.mtcomm.2019.100730

(45) Jiang L., Quannan W., Ping W., Hongmei W., Yong-Gui Z., Zhengkun Y., Transition-metal mediated carbon–sulfur bond activation and transformations: an update. *Chem. Soc. Rev.* **2020**; 49 (13): 4307–4359. https://doi.org/10.1039/c9cs00837c

(46) Rezvani M. A., Bakhtiyari A., Rahmani P., Synthesis and characterization of new nanocomposite PW11Mn@CuO@PANI as an efficient nanocatalyst for deep oxidative desulfurization of real/model fuels, *Mat. Sci. Eng.* B **2024**, 303, 117314. https://doi.org/10.1016/j.mseb.2024.117314.

Graphical Abstract

